Counterfactual quantum cloning without transmitting any physical particles

Qi Guo,[1,*] Shuqin Zhai,[1] Liu-Yong Cheng,[2] Hong-Fu Wang,[3] and Shou Zhang[3]
[1]*College of Physics and Electronic Engineering, Shanxi University, Taiyuan, Shanxi 030006, People's Republic of China*
[2]*College of Physics and Information Engineering, Shanxi Normal University, Linfen, Shanxi 041000, People's Republic of China*
[3]*Department of Physics, College of Science, Yanbian University, Yanji, Jilin 133002, People's Republic of China*
(Received 1 August 2017; published 27 November 2017)

We propose a counterfactual $1 \rightarrow 2$ economical phase-covariant cloning scheme. Compared with the existing protocols using flying qubits, the main difference of the presented scheme is that the cloning can be achieved without transmitting the photon between the two parties. In addition, this counterfactual scheme does not need to construct controlled quantum gates to perform joint logical operations between the cloned qubit and the blank copy. We also numerically evaluate the performance of the present scheme in the practical experiment, which shows this cloning scheme can be implemented with a high success of probability and the fidelity is close to the optimal value in the ideal asymptotic limit.

DOI: 10.1103/PhysRevA.96.052335

I. INTRODUCTION

Many counterintuitive effects in quantum mechanics provide powerful tools for quantum information processing [1]. Meanwhile, the development of quantum information also proves these quantum effects directly or indirectly, such as quantum nonlocality, complementarity, and so on. In recent years, counterfactual quantum information processing and quantum cryptography based on interaction-free measurement [2,3] and the chained quantum Zeno effect [4] have been studied extensively [5–11]. These works suggested some nonlocal quantum information tasks can be achieved without exchanging physical particles between two distant parties, which makes more and more people pay attention to the counterfactuality in quantum mechanics. In 2013, Salih *et al.* [9] showed that classical communication can be implemented without any particles traveling between the sender and the receiver, which challenged the longstanding assumption that information transfer relies on the transmission of physical particles. This work attracted much attention and gave rise to deep discussion about quantum counterfactuality [12–15]. Inspired by Salih's scheme, we generalized the counterfactual communication to the quantum situation and proved an unknown qubit can be teleported without transmitting physical particles [16]. Subsequently, Li *et al.* improved our scheme to increase the success probability to 100% [17]. Very recently, Cao *et al.* experimentally demonstrated the counterfactual communication by transferring a monochrome bitmap using a single photon source [18].

Quantum no-cloning theorem, proposed in 1982 by Wooters and Zurek [19], is another well-known property of quantum mechanics, which suggests that it is impossible to accurately clone an arbitrary quantum state for linearity of quantum mechanics. Nevertheless, whether an unknown or partially unknown quantum state can be cloned probabilistically or approximately became a focus of concern for physicists [20,21]. During the past two decades, different types of approximate quantum cloning have been intensively studied, such as universal quantum cloning [22–25] and phase-covariant cloning [26–30]. Duan and Guo proved that exact copying can be realized probabilistically for the input quantum state chosen from a subset of linear independent states [31].

Each type of quantum cloning protocol has its own characteristics. Phase-covariant cloning has a higher fidelity than the universal cloning due to exploiting a partial priori knowledge of the input state [26–30]. In original phase-covariant cloning schemes, the ancillas play a crucial role and make the quantum networks complex. For simplification, economical cloning without ancillas has been proposed [32] and studied widely in theory [33–40] and experiment [41–45] in recent years. Usually, in order to implement economical phase-covariant cloning scheme, one should first design a corresponding quantum logical network using single- and two-qubit quantum gates, and then use suitable physical systems to realize these quantum logical gates [46–53]. The schemes based on a flying qubit can implement the cloning among distant quantum nodes by transmitting the flying qubit [46–48,51,52]. Given the success of the counterfactual quantum communication, it may be a interesting issue whether the quantum cloning using a flying qubit can be achieved without transmitting the flying qubit between two parties.

Here we will explore the way to implement the quantum cloning based on counterfactual quantum communication and construct a counterfactual scheme for $1 \rightarrow 2$ economical phase-covariant cloning between the sender Alice and the receiver Bob, which demonstrates that quantum cloning with flying qubits can be achieved without transmitting any physical particles. This scheme does not require a controlled quantum gate between the qubit to be cloned and the blank copy. Moreover, during the whole process of the counterfactual quantum cloning, any other qubits are not needed besides the qubit to be cloned and the blank copy.

II. COUNTERFACTUAL $1 \rightarrow 2$ ECONOMICAL PHASE-COVARIANT CLONING SCHEME

One of the important modules in counterfactual quantum information processing is the quantum control device for the photon path, i.e., the absorption or passing of a photon in a transmission channel depends on a two-dimensional

*qguo@sxu.edu.cn

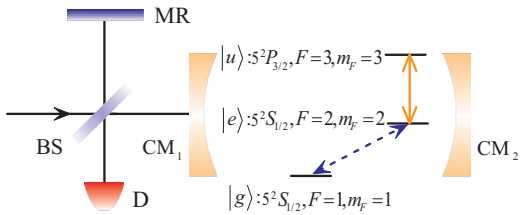

FIG. 1. The quantum control device for the photon path. MR: normal mirror; BS: 50:50 beam splitter; D: conventional photon detector; CM_1 and CM_2 compose a single-side cavity.

quantum superposition state. Many quantum phenomena can be used to construct such a device. For clarity, here we choose the atom-cavity quantum electrodynamics system as in Ref. [17] to illuminate the counterfactual quantum cloning. The schematic diagram of the photon-path control device can be represented as Fig. 1. A single ^{87}Rb atom is trapped at the center of a single-side cavity composed of CM_1 and CM_2. This atom-photon interaction mechanism has been extensively studied theoretically [54,55] and experimentally [56,57]. We select the states of the ^{87}Rb atom $|5^2S_{1/2},F=1,m_F=1\rangle$, $|5^2S_{1/2},F=2,m_F=2\rangle$, and $|5^2P_{3/2},F=3,m_F=3\rangle$ as the ground state $|g\rangle$, the lower excited state $|e\rangle$, and the upper excited state $|u\rangle$, respectively. The cavity is resonant with the transition between the states $|e\rangle$ and $|u\rangle$, and the transition $|g\rangle \leftrightarrow |e\rangle$ is driven by a pair of Raman lasers [56,58]. As shown in Refs. [56,57], when a photon which is resonant with the empty cavity interacts with the atom-cavity system, it experiences a phase shift depending on the coupling strength. If the atom is in the state $|g\rangle$, it will not interact with the photon. Thus, the photon will enter the cavity and then be reflected with a π phase shift. However, if the atom is in the state $|e\rangle$, the strong atom-photon coupling leads to a normal-mode splitting [59], so that the photon is directly reflected without π phase shift. In order to achieve the quantum control to the photon, a 50:50 beam splitter (BS) and a mirror (MR) are added outside the cavity to form a Michelson interferometer [17]. Therefore, for the atom state $|g\rangle$, the incoming photon will be reflected with a π phase shift and then be absorbed by the detector D; however, for the state $|e\rangle$, the photon will return back to the input port. That is, the absorption or passing of the photon in the path is controlled by the quantum state of the atom.

We now discuss how to achieve the counterfactual $1 \to 2$ economical phase-covariant cloning. Assume that Alice wants to clone the state of her photon to Bob's atom. We first introduce the cloning of an unknown state on the northern hemispheres of the Bloch sphere. The schematic diagram of the cloning machine is shown in Fig. 2. The main part of the setup is a nested Michelson-type interferometer. The two optical paths from the switchable mirror SM_1 to the normal mirror MR_1 i.e., $SM_1 \to MR_1$ and $SM_1 \to$ cavity, form the outer Michelson-type interferometer, and the two optical paths $SM_2 \to MR_2$ and $SM_2 \to$ cavity form the inner Michelson-type interferometer inserted in one of the arms of the outer interferometer. Alice's photon state to be cloned is in an arbitrary state on the northern hemispheres, and Bob's atom is initially in $|g\rangle$ as a blank copy. Thus, the joint initial state is

$$|\psi\rangle_0 = \left(\cos\frac{\theta}{2}|H\rangle + e^{i\varphi}\sin\frac{\theta}{2}|V\rangle\right)|g\rangle, \tag{1}$$

where $|H\rangle$ and $|V\rangle$, respectively, denote the horizontal polarization and vertical polarization state of Alice's photon, and $\theta \in [0,\pi/2], \varphi \in [0,2\pi]$. First, Bob performs a transformation $|g\rangle \to (1/\sqrt{2})(|g\rangle + |e\rangle)$ on his atom with a driving laser field. Meanwhile, Alice's photon passes through the polarizing beam splitter PBS_1 and the $|H\rangle$ component goes to the optical delay

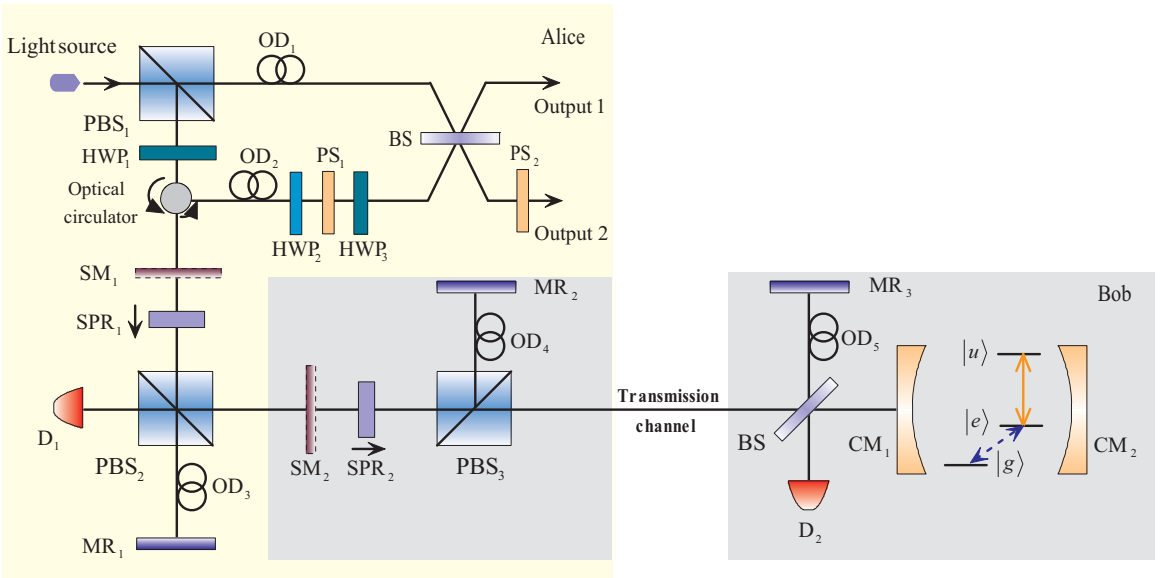

FIG. 2. Schematic of the counterfactual $1 \to 2$ economical phase-covariant cloning. PBS_k ($k = 1,2,3$): polarizing beam splitter; $SM_{1(2)}$: switchable mirror; $SPR_{1(2)}$: switchable polarization rotator, where the arrow means $SPR_{1(2)}$ can rotate only the photon coming from the $SM_{1(2)}$ side; $D_{1(2)}$: conventional photon detector; $HWP_{1(3)}$: half-wave plate oriented at 45°; HWP_2: half-wave plate oriented at 22.5°; PS: phase shifter; BS: 50:50 beam splitter; OD: optical delay line.

line OD_1, while the $|V\rangle$ component undergoes a transformation $|V\rangle \to |H\rangle$ by the half-wave plate HWP_1 oriented at 45°. Hence, the initial state becomes

$$|\psi\rangle_0 \to \frac{1}{\sqrt{2}}\cos\frac{\theta}{2}|H\rangle_1(|g\rangle + |e\rangle) + \frac{1}{\sqrt{2}}e^{i\varphi}\sin\frac{\theta}{2}|H\rangle_2(|g\rangle + |e\rangle), \quad (2)$$

where the subscripts indicate the two paths.

Clearly, only the second term in Eq. (2) will enter into the nested interferometer. For the sake of simplicity, we consider only the evolution of the component $|\phi\rangle \equiv \frac{1}{\sqrt{2}}|H\rangle_2(|g\rangle + |e\rangle)$ in Eq. (2) for the moment. Then $|H\rangle_2$ enters the nested interferometer via the optical circulator. The SM_1 is initially switched off to allow the photon to be transmitted, but it remains on (reflects the photon) once the photon enters the interferometer until the photon finishes M cycles in the outer interferometer. The switchable polarization rotator SPR_1 will rotate only the photon coming from SM_1 by an angle β_1 ($\beta_1 = \pi/2M$), i.e., $|H\rangle \to \cos\beta_1|H\rangle + \sin\beta_1|V\rangle$ and $|V\rangle \to \cos\beta_1|V\rangle - \sin\beta_1|H\rangle$. After passing through SPR_1, $|\phi\rangle$ evolves as

$$|\phi\rangle \to \frac{1}{\sqrt{2}}(\cos\beta_1|H\rangle + \sin\beta_1|V\rangle)(|g\rangle + |e\rangle) = \frac{1}{\sqrt{2}}\cos\beta_1|H\rangle(|g\rangle + |e\rangle) + \frac{1}{\sqrt{2}}\sin\beta_1|V\rangle(|g\rangle + |e\rangle). \quad (3)$$

Due to PBS_2, only the component $|V\rangle$ can enter the inner interferometer. Therefore, we can take the component $|\chi\rangle \equiv \frac{1}{\sqrt{2}}|V\rangle(|g\rangle + |e\rangle)$ from Eq. (3) to introduce the action of the inner interferometer. The SM_2, similarly to SM_1, can transmit photons initially, and after a photon enters the inner interferometer, it keeps reflecting the photon until the photon finishes the Nth inner cycle. The action of SPR_2 is similar to SPR_1, only rotating the photon coming from SM_2 by an angle β_2 ($\beta_2 = \pi/2N$). After passing through SPR_2, $|\chi\rangle$ evolves as

$$|\chi\rangle \to \frac{1}{\sqrt{2}}(\cos\beta_2|V\rangle - \sin\beta_2|H\rangle)(|g\rangle + |e\rangle). \quad (4)$$

Then the photon passes through PBS_3, and the component $|V\rangle$ travels to MR_2, while the component $|H\rangle$ enters the transmission channel to meet Bob's quantum control device. According to the mechanism of Bob's device discussed above, if the atom is in the state $|g\rangle$, the incoming photon will be absorbed by detector D_2. Thus, if the photon is not absorbed by D_2, it will go back to SM_2 and finish the first inner cycle, and the state becomes

$$|\chi\rangle \to \frac{1}{\sqrt{2}}\cos\beta_2|V\rangle(|g\rangle + |e\rangle) - \frac{1}{\sqrt{2}}\sin\beta_2|H\rangle|e\rangle. \quad (5)$$

Equation (5) is obtained by ignoring the component $|H\rangle|g\rangle$ in Eq. (4), because the photon will be absorbed for the atom state $|g\rangle$. Therefore, Eq. (5) is not normalized. If the photon is never absorbed by D_2 during the N cycles in the inner interferometer, the state at the end of the Nth inner cycle can be straightforwardly obtained:

$$|\chi\rangle \to \frac{1}{\sqrt{2}}[\cos^N\beta_2|V\rangle|g\rangle + \cos(N\beta_2)|V\rangle|e\rangle - \sin(N\beta_2)|H\rangle|e\rangle]. \quad (6)$$

By setting $\beta_2 = \frac{\pi}{2N}$, the equation above becomes

$$|\chi\rangle \to \frac{1}{\sqrt{2}}\left(\cos^N\frac{\pi}{2N}|V\rangle|g\rangle - |H\rangle|e\rangle\right). \quad (7)$$

Substituting this evolved $|\chi\rangle$ into Eq. (3), we can obtained the final state of $|\phi\rangle$ after the N inner cycles:

$$|\phi\rangle \to \frac{1}{\sqrt{2}}\cos\beta_1|H\rangle(|g\rangle + |e\rangle) + \frac{1}{\sqrt{2}}\sin\beta_1\left(\cos^N\frac{\pi}{2N}|V\rangle|g\rangle - \underline{|H\rangle|e\rangle}\right). \quad (8)$$

When the photon component finishes N inner cycles and goes out of the inner interferometer, it will combine with the component from MR_1 by PBS_2. The underline in Eq. (8) means that the $|H\rangle$ component from the inner interferometer will be absorbed by the detector D_1, while other components will return to SM_1, and the first outer cycle is finished. Therefore, if the photon isn't absorbed by D_1 or D_2, at the end of the first outer cycle, $|\phi\rangle$ evolves to

$$|\phi\rangle \to \frac{1}{\sqrt{2}}\cos\beta_1|H\rangle(|g\rangle + |e\rangle) + \frac{1}{\sqrt{2}}\sin\beta_1\cos^N\frac{\pi}{2N}|V\rangle|g\rangle. \quad (9)$$

Then continue the 2th–Mth outer cycles. In the case that the photon is never absorbed by D_1 or D_2 during the M outer cycles, $|\phi\rangle$ becomes

$$|\phi\rangle \to \frac{1}{\sqrt{2}}x_M|V\rangle|g\rangle - \frac{1}{\sqrt{2}}y_M|H\rangle|g\rangle + \frac{1}{\sqrt{2}}z_M|H\rangle|e\rangle, \quad (10)$$

where the coefficients x_M, y_M, and z_M satisfy the recursion relations

$$x_M = (x_{M-1}\cos\beta_1 - y_{M-1}\sin\beta_1)\cos^N\frac{\pi}{2N},$$
$$y_M = (x_{M-1}\sin\beta_1 + y_{M-1}\cos\beta_1),$$
$$z_M = z_{M-1}\cos\beta_1, \quad (11)$$

with $x_0 = 0$, $y_0 = -1$, and $z_0 = 1$. Then the photon leaves the outer interferometer and enters OD_2 via SM_1 and the optical circulator successively. Now, replacing the component $\frac{1}{\sqrt{2}}|H\rangle_2(|g\rangle + |e\rangle)$ in Eq. (2) with the evolved $|\phi\rangle$ in Eq. (10), we can obtain the joint state evolved by the nested interferometer

$$|\psi\rangle_M = \frac{1}{\sqrt{2}}\cos\frac{\theta}{2}|H\rangle_1(|g\rangle + |e\rangle) + \frac{1}{\sqrt{2}}e^{i\varphi}\sin\frac{\theta}{2}(x_M|V\rangle_2|g\rangle - y_M|H\rangle_2|g\rangle + z_M|H\rangle_2|e\rangle). \quad (12)$$

Then perform Hadamard transformations on the atom and the component of the photon in path 2, respectively, by using the driving laser field and HWP_2, i.e., $\{|g\rangle \to (1/\sqrt{2})(|g\rangle + |e\rangle)$,

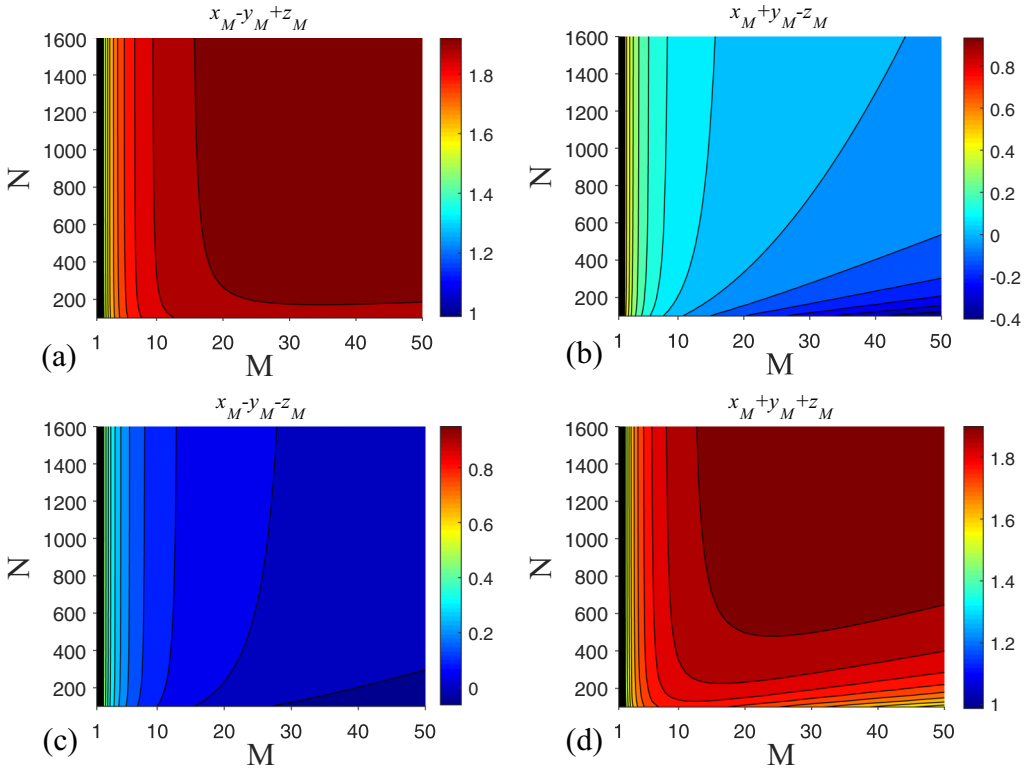

FIG. 3. The parameters $x_M - y_M + z_M$, $x_M + y_M - z_M$, $x_M - y_M - z_M$, and $x_M + y_M + z_M$ in Eq. (13) versus the different values of N and M. (a) $x_M - y_M + z_M$ is close to 2, (b) $x_M + y_M - z_M$ approaches to 0, (c) $x_M - y_M - z_M$ is close to 0, (d) $x_M + y_M + z_M$ tends to 2 for large N and M.

$|e\rangle \to (1/\sqrt{2})(|g\rangle - |e\rangle)\}$, and $\{|H\rangle \to (1/\sqrt{2})(|H\rangle + |V\rangle)$, $|V\rangle \to (1/\sqrt{2})(|H\rangle - |V\rangle)\}$. The whole state becomes

$$|\psi\rangle_M \to \cos\frac{\theta}{2}|H\rangle_1|g\rangle + \frac{1}{2\sqrt{2}}e^{i\varphi}\sin\frac{\theta}{2}\{[(x_M-y_M+z_M)|H\rangle_2 - (x_M+y_M-z_M)|V\rangle_2]|g\rangle + [(x_M-y_M-z_M)|H\rangle_2-(x_M+y_M+z_M)|V\rangle_2]|e\rangle\}. \quad (13)$$

For clarity, we numerically analyze the variation trend of the coefficients above with the values of N and M, as shown in Fig. 3. It can be seen that, with the increase of N and M, $(x_M - y_M + z_M) \to 2$, $(x_M + y_M - z_M) \to 0$, $(x_M - y_M - z_M) \to 0$, $(x_M + y_M + z_M) \to 2$. Therefore, for large values of N and M, the state in Eq. (13) can be approximately written as

$$|\psi\rangle_M \to \cos\frac{\theta}{2}|H\rangle_1|g\rangle + \frac{1}{\sqrt{2}}e^{i\varphi}\sin\frac{\theta}{2}(|H\rangle_2|g\rangle - |V\rangle_2|e\rangle). \quad (14)$$

The action of the phase shifter $PS_{1(2)}$ and the half-wave plate HWP_3 oriented at 45° is to perform the transformations $\{|H\rangle \to |H\rangle, |V\rangle \to -|V\rangle\}$ and $\{|H\rangle \to |V\rangle, |V\rangle \to |H\rangle\}$, respectively. Therefore, after passing through PS_1 and HWP_3, the state becomes

$$|\psi\rangle_M \to \cos\frac{\theta}{2}|H\rangle_1|g\rangle + \frac{1}{\sqrt{2}}e^{i\varphi}\sin\frac{\theta}{2}(|V\rangle_2|g\rangle + |H\rangle_2|e\rangle). \quad (15)$$

Then after the photon passes through BS and PS_2 on path 2, the state will evolve to

$$|\psi\rangle_M \to \frac{1}{\sqrt{2}}\left[\cos\frac{\theta}{2}|H\rangle_1|g\rangle+\frac{1}{\sqrt{2}}e^{i\varphi}\sin\frac{\theta}{2}(|V\rangle_1|g\rangle+|H\rangle_1|e\rangle)\right] + \frac{1}{\sqrt{2}}\left[\cos\frac{\theta}{2}|H\rangle_2|g\rangle+\frac{1}{\sqrt{2}}e^{i\varphi}\sin\frac{\theta}{2}(|V\rangle_2|g\rangle-|H\rangle_2|e\rangle)\right]. \quad (16)$$

Performing a nondestructive detection [56] of the photon on the two paths, if the photon is in path 1, the state above will collapse to

$$|\psi\rangle_M \to \cos\frac{\theta}{2}|H\rangle|g\rangle + \frac{1}{\sqrt{2}}e^{i\varphi}\sin\frac{\theta}{2}(|V\rangle|g\rangle + |H\rangle|e\rangle). \quad (17)$$

This is the desired state of an optimal $1 \to 2$ economical phase-covariant cloning for the state on the northern hemispheres of the Bloch sphere.

If the photon is in path 2, the state in Eq. (16) will collapse to

$$|\psi\rangle_M \to \cos\frac{\theta}{2}|H\rangle|g\rangle + \frac{1}{\sqrt{2}}e^{i\varphi}\sin\frac{\theta}{2}(|V\rangle|g\rangle - |H\rangle|e\rangle). \quad (18)$$

Bob performs a σ_z operation on the atom by using the driving laser field, i.e., $\{|g\rangle \to |g\rangle, |e\rangle \to -|e\rangle\}$. Then we can obtain

the same state as Eq. (17). In this case, it should be pointed out that Alice needs to send the detection result (1 bit of classical information) to Bob by the counterfactual manner in Ref. [9]. Therefore, the cloning scheme can be achieved regardless of which path the photon is in.

During the whole cloning process from Eq. (1) to Eq. (17), we can see the photon has never passed through the transmission channel and never gotten to Bob's site. That is because once the photon passed through the channel, it will be absorbed by D_1 or D_2. Hence, as long as the photon can achieve the output port at the end, it shows that the photon has not entered the channel and the counterfactual quantum cloning is completed. In the next section, we will show that the probability that the photon enters the transmission channel can be strongly suppressed by repeatedly using the nested interferometer, and the counterfactual cloning scheme can be achieved with a high success of probability.

The counterfactual quantum cloning for the state on the southern hemispheres of the Bloch sphere can also be achieved by making slight changes to the setup in Fig. 2. To this end, we choose the initial state with the same form as Eq. (1), but $\theta \in [\pi/2,\pi]$ and $\varphi \in [0,2\pi]$. Remove HWP_1 and inject the photon from the top of PBS_1, i.e., the $|H\rangle$ component enters into the nested interferometer directly, while $|V\rangle$ component goes to the optical delay line OD_1. Then perform the same process as that from Eq. (2) to Eq. (17), we can obtain the final state

$$|\psi\rangle'_M \rightarrow \frac{1}{\sqrt{2}}\cos\frac{\theta}{2}(|V\rangle|g\rangle + |H\rangle|e\rangle) + e^{i\varphi}\sin\frac{\theta}{2}|V\rangle|e\rangle, \tag{19}$$

which is the desired state of $1 \rightarrow 2$ economical phase-covariant cloning for the state on the southern hemispheres of the Bloch sphere. It can also be proved that the photon never enters the transmission channel. Therefore, now, we have showed that the economical phase-covariant cloning for an arbitrary quantum state can be achieved counterfactually.

III. DISCUSSION AND CONCLUSIONS

The counterfactual quantum cloning described above is accomplished under the ideal experimental conditions and the extreme situation of $N,M \rightarrow \infty$. However, in the practical experiment, N and M must be finite, and some influence factors should be considered. In this section, we will numerically analyze the effect of these factors on the performance of the present scheme and discuss the experimental feasibility under the practical conditions. It is worth emphasizing that, as long as the quantum control device for the photon path can be implemented, the present counterfactual scheme is universal for other physical systems, and it has been explained by using the cavity input-output process in this paper. Though this system does not need the single-photon absorbtion by one atom that is hard to realize, the strong coupling between the cavity and the transition $|e\rangle \leftrightarrow |u\rangle$ is required. The interaction mechanism of the input-output process has been widely researched [54–57]. In particular, the experiment in Ref. [56] shows that the probability of getting a reflected photon from the single-photon input-output process can reach 66%, and the probability can be further improved by utilizing a whispering-gallery-mode microresonator [60]. The detailed discussion has been given in the references. In the following, we will analyze several other important factors in detail.

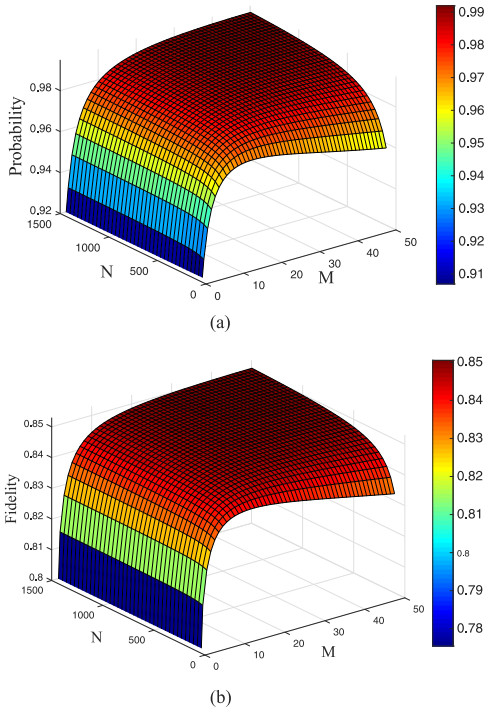

FIG. 4. The average success probability (a) and the average fidelity (b) of the counterfactual cloning scheme versus different values of outer and inner cycles M and N.

The key optical elements in the present scheme are the two switchable polarization rotators SPR_1 and SPR_2 with suitable angles β_1 and β_2 that depend on the values of inner and outer cycles N and M. From the above discussion, we can see the cloning scheme can be achieved approximately with $N,M \rightarrow \infty$. Therefore, the values of N and M will directly affect the performance of the scheme, and we here first analyze the influence from N and M. Take the state on the northern hemispheres of the Bloch sphere, for example; thus, we can evaluate the effect of N and M on the successful probability and fidelity of the whole scheme via Eq. (13). Fidelity is an important index for evaluating quantum cloning machines, and the optimal fidelity for economical phase-covariant cloning is 0.854 [33]. Because the exact information of the cloned state is unknown, the successful probability and fidelity must be functions of θ [denoted as $P(\theta)$ and $F(\theta)$, respectively]. Therefore, we use the average successful probability and the average fidelity to quantitatively analyze the performance of the cloning scheme, i.e., $\overline{P} = \frac{2}{\pi}\int_0^{\pi/2} P(\theta)\,d\theta$ and $\overline{F} = \frac{2}{\pi}\int_0^{\pi/2} F(\theta)\,d\theta$. We numerically evaluate the average success probability and fidelity with different N and M in Fig. 4(a) and Fig. 4(b). It is obvious that the average success probability tends to 1, and the average fidelity tends to the optimal fidelity with the increase of N and M. For example, $\overline{P} = 0.9873$ and $\overline{F} = 0.8485$ for $N = 600$ and $M = 30$, and $\overline{P} = 0.9919$ and $\overline{F} = 0.8505$ for $N = 1500$ and $M = 50$. Hence, the large values of N and M can suppress the probability the the photon passes through the channel, and the present counterfactual

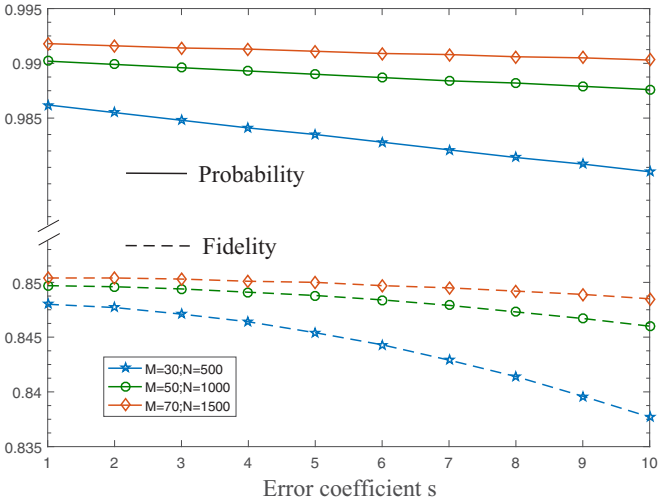

FIG. 5. The average successful probability (solid lines) and the average fidelity (dotted lines) versus the error coefficient s of the SPR for the different values of M and N.

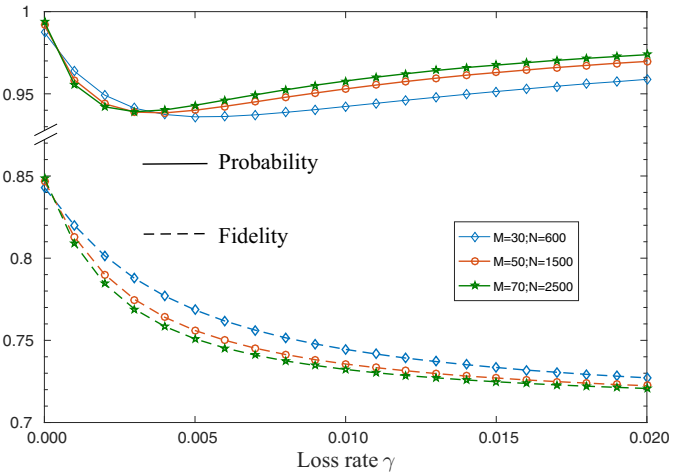

FIG. 6. The average successful probability (solid lines) and the average fidelity (dotted lines) versus the photon loss probability γ in the transmission channel for the different values of M and N.

scheme can be close to the optimal economical phase-covariant cloning.

The two switchable polarization rotators are required to have the high-precision rotation angles $\beta_1 = \pi/(2M)$ and $\beta_2 = \pi/(2N)$. However, it is bound to introduce slight errors in the practical situations. In order to analyze the influence from the inaccuracy of $\mathrm{SPR}_{1(2)}$, we suppose the error coefficient of $\mathrm{SPR}_{1(2)}$ is $s_{1(2)}$, which means when a photon passes through $\mathrm{SPR}_{1(2)}$ the rotation angle has a error $\Delta\beta_1 = s_1\beta_1/M$ ($\Delta\beta_2 = s_2\beta_2/M$). Then, by replacing $\beta_{1(2)}$ with $\beta_{1(2)} + \Delta\beta_{1(2)}$ during the cloning process, we can obtain the final state involving $s_{1(2)}$. For convenience, we assume SPR_1 and SPR_2 have the same error coefficient, $s_1 = s_2 = s$. In Fig. 5 we plot the average successful probability (solid lines) and the average fidelity (dotted lines) versus the error coefficient for different values of M and N, which indicates both the successful probability and the average fidelity decrease with the increase of s. Fortunately, the decay due to s can be compensated by increasing the numbers of inner and outer cycles N and M.

Next, we analyze the influence of the photon loss in the transmission channel. The photon loss rate γ can be defined as the probability that the photon is absorbed by other unexpected objects in the transmission channel in every cycle rather than the detectors. After considering the loss, we need to rederive the counterfactual cloning process, and the coefficient of the component $|H\rangle|e\rangle$ in Eq. (5) will change to $-\frac{1}{\sqrt{2}}(1-\gamma)\sin\beta_2$. With lengthy calculations, we can obtain the final state containing γ. We also use the average successful probability and the average fidelity to evaluate the effect of the photon loss. The numerical analysis results for different values of γ, M, and N is shown in Fig. 6. It can be found that the average successful probabilities decrease first and then increase slightly with the increase of γ. That is because Alice's end cannot distinguish when a photon is absorbed by D_2 (Bob's atom in $|g\rangle$) or by other unexpected objects. In other words, when the photon loss is present and the atom is in $|e\rangle$, one can still obtain the same result as the case that the atom is in $|g\rangle$. Specifically, from Eq. (14), we can see if Bob's atom is in $|g\rangle$, Alice's output 2 will obtain $|H\rangle$ polarization. However, if the photon loss is present, even though Bob's atom is in $|e\rangle$, the output 2 will obtain $|H\rangle$ polarization incorrectly. In this case, the scheme appears to be success, but the fidelity will decay. Therefore, as shown in Fig. 6, the fidelity always decreases. Moreover, with the increase of M and N, the successful probability increases, while the fidelity decreases.

In summary, we have proposed a counterfactual $1 \to 2$ economical phase-covariant cloning scheme, which demonstrated that quantum cloning using flying qubits can be achieved without transmitting any physical particles. This counterfactual scheme was based on the interaction-free measurement and didn't need to construct a complex quantum network for performing joint logical operations between the cloned qubit and the blank copy. The numerical analysis of the effect of relevant influence factors in the practical situations showed the scheme can be accomplished with a high probability of success and fidelity. Therefore, the counterfactual cloning scheme is effective and perhaps opens promising possibilities for quantum cloning.

ACKNOWLEDGMENTS

This work is supported by the National Natural Science Foundation of China under Grants No. 11604190, No. 61465013, No. 11264042, No. 11465020, and No. 11704235 and the Fund for Shanxi "1331 Project" Key Subjects Construction.

[1] M. A. Nielsen and I. L. Chuang, *Quantum Computation and Quantum Information* (Cambridge University Press, Cambridge, 2000).

[2] A. C. Elitzur and L. Vaidman, Found. Phys. **23**, 987 (1993).

[3] P. Kwiat, H. Weinfurter, T. Herzog, A. Zeilinger, and M. A. Kasevich, Phys. Rev. Lett. **74**, 4763 (1995).

[4] P. G. Kwiat, A. G. White, J. R. Mitchell, O. Nairz, G. Weihs, H. Weinfurter, and A. Zeilinger, Phys. Rev. Lett. **83**, 4725 (1999).
[5] O. Hosten, M. T. Rakher, J. T. Barreiro, N. A. Peters, and P. G. Kwiat, Nature (London) **439**, 949 (2006).
[6] T.-G. Noh, Phys. Rev. Lett. **103**, 230501 (2009).
[7] Y. Liu, L. Ju, X. L. Liang, S. B. Tang, G. L. Shen Tu, L. Zhou, C. Z. Peng, K. Chen, T. Y. Chen, Z. B. Chen, and J. W. Pan, Phys. Rev. Lett. **109**, 030501 (2012).
[8] Z. Q. Yin, H. W. Li, Y. Yao, C. M. Zhang, S. Wang, W. Chen, G. C. Guo, and Z. F. Han, Phys. Rev. A **86**, 022313 (2012).
[9] H. Salih, Z. H. Li, M. Al-Amri, and M. S. Zubairy, Phys. Rev. Lett. **110**, 170502 (2013).
[10] N. Gisin, Phys. Rev. A **88**, 030301 (2013).
[11] J. L. Zhang, F. Z. Guo, F. Gao, B. Liu, and Q. Y. Wen, Phys. Rev. A **88**, 022334 (2013).
[12] L. Vaidman, Phys. Rev. Lett. **112**, 208901 (2014).
[13] H. Salih, Z. H. Li, M. Al-Amri, and M. S. Zubairy, Phys. Rev. Lett. **112**, 208902 (2014).
[14] L. Vaidman, J. Phys. A: Math. Theor. **48**, 465303 (2015).
[15] D. R. M. Arvidsson-Shukur and C. H. W. Barnes, arXiv:1705.06574 (2017).
[16] Q. Guo, L. Y. Cheng, L. Chen, H. F. Wang, and S. Zhang, Sci. Rep. **5**, 8416 (2015).
[17] Z. H. Li, M. Al-Amri, and M. S. Zubairy, Phys. Rev. A **92**, 052315 (2015).
[18] Y. Cao, Y.-H. Li, Z. Cao, J. Yin, Y.-A. Chen, H.-L. Yin, T.-Y. Chen, X. Ma, C.-Z. Peng, and J.-W. Pan, Proc. Natl. Acad. Sci. USA **114**, 4920 (2017).
[19] W. K. Wootters and W. H. Zurek, Nature (London) **299**, 802 (1982).
[20] V. Scarani, S. Iblisdir, N. Gisin, and A. Acín, Rev. Mod. Phys. **77**, 1225 (2005).
[21] H. Fan, Y. N. Wang, L. Jing, J. D. Yue, H. D. Shi, Y. L. Zhang, and L. Z. Mu, Phys. Rep. **544**, 241 (2014).
[22] V. Buzěk and M. Hillery, Phys. Rev. A **54**, 1844 (1996).
[23] N. Gisin and S. Massar, Phys. Rev. Lett. **79**, 2153 (1997).
[24] R. F. Werner, Phys. Rev. A **58**, 1827 (1998).
[25] V. Buzěk and M. Hillery, Phys. Rev. Lett. **81**, 5003 (1998).
[26] D. Bruß, M. Cinchetti, G. M. D'Ariano, and C. Macchiavello, Phys. Rev. A **62**, 012302 (2000).
[27] P. Navez and N. J. Cerf, Phys. Rev. A **68**, 032313 (2003).
[28] W. H. Zhang, T. Wu, L. Ye, and J. L. Dai, Phys. Rev. A **75**, 044303 (2007).
[29] A. Zhu, K. H. Yeon, and S. C. Yu, J. Phys. B **42**, 235501 (2009).
[30] H. Fan, H. Imai, K. Matsumoto, and X. B. Wang, Phys. Rev. A **67**, 022317 (2003).
[31] L. M. Duan and G. C. Guo, Phys. Rev. Lett. **80**, 4999 (1998).
[32] C.-S. Niu and R. B. Griffiths, Phys. Rev. A **60**, 2764 (1999).
[33] J. Fiurášek, Phys. Rev. A **67**, 052314 (2003).
[34] T. Durt and J. F. Du, Phys. Rev. A **69**, 062316 (2004).
[35] F. Buscemi, G. M. D'Ariano, and C. Macchiavello, Phys. Rev. A **71**, 042327 (2005).
[36] Y. Dong, X. Zou, S. Li, and G. Guo, Phys. Rev. A **76**, 014303 (2007).
[37] T. Durt, J. Fiurášek, and N. J. Cerf, Phys. Rev. A **72**, 052322 (2005).
[38] W.-H. Zhang, L.-B. Yu, L. Ye, and J.-L. Dai, Phys. Lett. A **360**, 726 (2007).
[39] X. Zou, Y. Dong, and G. Guo, Phys. Lett. A **360**, 44 (2006).
[40] N. J. Cerf, Phys. Rev. Lett. **84**, 4497 (2000).
[41] I. Ali Khan and J. C. Howell, Phys. Rev. A **70**, 010303(R) (2004).
[42] J. F. Du, T. Durt, P. Zou, H. Li, L. C. Kwek, C. H. Lai, C. H. Oh, and A. Ekert, Phys. Rev. Lett. **94**, 040505 (2005).
[43] J.-S. Xu, C.-F. Li, L. Chen, X.-B. Zou, and G.-C. Guo, Phys. Rev. A **78**, 032322 (2008).
[44] J. Soubusta, L. Bartůškova, A. Černoch, M. Dušek, and J. Fiurášek, Phys. Rev. A **78**, 052323 (2008).
[45] K. Lemr, K. Bartkiewicz, A. Černoch, J. Soubusta, and A. Miranowicz, Phys. Rev. A **85**, 050307(R) (2012).
[46] X. B. Zou and W. Mathis, Phys. Rev. A **72**, 022306 (2005).
[47] X. B. Zou, K. Li, and G. C. Guo, Phys. Lett. A **366**, 36 (2007).
[48] L. Ye, W. Xiong, A. X. Li, and G. C. Guo, Sci. China, Phys. Mech. Astron. **54**, 262 (2011).
[49] L. B. Yu, W. H. Zhang, and L. Ye, Phys. Rev. A **76**, 034303 (2007).
[50] B. L. Fang, Z. Yang, and L. Ye, Phys. Rev. A **79**, 054308 (2009).
[51] F. Sciarrino and F. De Martini, Phys. Rev. A **76**, 012330 (2007).
[52] Z. Jin, Y.-Q. Ji, A.-D. Zhu, H.-F. Wang, and S. Zhang, Opt. Commun. **315**, 265 (2014).
[53] G. M. D'Ariano, C. Macchiavello, and M. Rossi, Phys. Rev. A **87**, 032337 (2013).
[54] L.-M. Duan and H. J. Kimble, Phys. Rev. Lett. **92**, 127902 (2004).
[55] J. Cho and H.-W. Lee, Phys. Rev. Lett. **95**, 160501 (2005).
[56] A. Reiserer, S. Ritter, and G. Rempe, Science **342**, 1349 (2013).
[57] A. Reiserer, N. Kalb, G. Rempe, and S. Ritter, Nature (London) **508**, 237 (2014).
[58] D. D. Yavuz, P. B. Kulatunga, E. Urban, T. A. Johnson, N. Proite, T. Henage, T. G. Walker, and M. Saffman, Phys. Rev. Lett. **96**, 063001 (2006).
[59] A. Boca, R. Miller, K. M. Birnbaum, A. D. Boozer, J. McKeever, and H. J. Kimble, Phys. Rev. Lett. **93**, 233603 (2004).
[60] C. Junge, D. O'Shea, J. Volz, and A. Rauschenbeutel, Phys. Rev. Lett. **110**, 213604 (2013).